Towards Understanding the Origin of Cosmic-Ray Electrons
- SUPPLEMENTAL MATERIAL -

(AMS Collaboration)

For references see the main text.

Detector.— The tracker accurately determines the particle trajectory and measures the rigidity R (momentum divided by charge), the charge $|Z|$ in elementary charge units, and the charge sign of cosmic rays by multiple measurements of the coordinates in the magnetic field and the particle energy loss in the silicon layers. The tracker has nine layers, the first $L1$ at the top of the detector, the second $L2$ above the magnet, six $L3$ to $L8$ within the bore of the magnet, and the last $L9$ above the ECAL. $L2$ to $L8$ constitute the inner tracker. For $|Z| = 1$ particles the maximum detectable rigidity, MDR, is 2 TV over the 3 m lever arm and the charge resolution is $\Delta Z = 0.05$. The TOF measures $|Z|$ with a resolution $\Delta Z = 0.05$ and velocity β with a resolution of $\Delta\beta/\beta^2 = 4\%$. The TRD separates electrons and positrons $e^{\pm}$ from protons p using a Λ_{TRD} estimator constructed from the ratio of the log–likelihood probability of the $e^{\pm}$ hypothesis to that of the p hypothesis in each layer [3]. The 3-dimensional imaging capability of the 17 radiation length ECAL allows for an accurate measurement of the $e^{\pm}$ energy and of the shower shape. An ECAL estimator Λ_{ECAL} [20] is used to differentiate $e^{\pm}$ from p by exploiting their different shower shapes. An illustration of the proton rejection as a function of momentum using the Λ_{ECAL} estimator is shown in Fig. S1.

The entire detector has been extensively calibrated in a test beam at CERN with e^+ and e^- from 10 to 290 GeV/c, with p at 180 and 400 GeV/c, and with π from 10 to 180 GeV/c, which produce transition radiation equivalent to p up to 1.2 TeV/c. Measurements with 18 different energies and particles at 2000 positions were performed. A Monte Carlo program, based on the GEANT4 10.1 package [22], is used to simulate physics processes and signals in the detector. It accurately describes the detector performance and has been verified using extensive calibrations both on the ground and on ISS up to much higher energies than presented in the Letter. Examples of thorough understanding of the detector performance, particularly at high energies, are presented in Figs. S2, S3 and S4.

Energy cutoff.— To investigate the existence of a finite energy cutoff in the electron flux, we use Eq. (4) to fit the data in the energy range energy range $[41.61 - 1400]$ GeV. The fit to data yields the inverse cutoff energy $1/E_s = 0.00^{+0.08}_{-0.00}\,\mathrm{TeV}^{-1}$, $C_s = (2.126 \pm 0.010) \times 10^{-3}[\mathrm{m}^2\,\mathrm{sr}\,\mathrm{s}\,\mathrm{GeV}]^{-1}$, $\gamma_s = -3.186^{+0.012}_{-0.006}$, and $\chi^2/\mathrm{d.o.f.} = 15.2/23$. The result of the fit shows the absence of the cutoff in the energy range below 1400 GeV as presented in Fig. S9. To study the significance of the $1/E_s$ measurement, we varied all three fit parameters in Eq. (4) to find the minimal $\Delta\chi^2$ corresponding to E_s values from 1 to 100 TeV. The blue curve in the insert shows the dependence of $\Delta\chi^2$ on E_s and the horizontal dashed lines show different significance levels from 1σ (black line), 2σ (green line), 3σ (blue line), 4σ (red line), and 5σ (magenta line, 99.9999% C.L.). As seen, E_s values below 1.9 TeV are excluded at the 5σ level.

Positron source term.— New sources of high energy positrons, such as dark matter, also produce an equal amount of high energy electrons [5, 7]. To test the consistency of this assumption with the data in the energy range $[41.61 - 1400]$ GeV, the electron flux is parametrized as a sum of a power law component and the identical source term as for positrons [4]:

$$\Phi_{e^-}(E) = C_{e^-}\,(E/E_1)^{\gamma_{e^-}} + f_{e^-}\,C_s^{e^+}(E/E_2)^{\gamma_s^{e^+}}\exp(-E/E_s^{e^+}). \tag{S1}$$

The power law component is characterized by the normalization factor C_{e^-} and the spectral index γ_{e^-}. The constant $E_1 = 41.61$ GeV corresponds to the beginning of the fit range, it does not affect the fitted value of γ_{e^-}. The values of the source term parameters $C_s^{e^+}$, $\gamma_s^{e^+}$, E_2, and $E_s^{e^+}$ are taken from Ref. [4]. A fit to the data with the source term normalization f_{e^-} fixed to 1 is performed in the energy range $[41.61 - 1400]$ GeV, where the solar modulation effects are negligible. It yields $C_{e^-} = (1.965 \pm 0.010) \times 10^{-3}\,[\mathrm{m}^2\,\mathrm{sr}\,\mathrm{s}\,\mathrm{GeV}]^{-1}$ and $\gamma_{e^-} = -3.248 \pm 0.007$ for the power law component with $\chi^2/\mathrm{d.o.f.} = 15.5/24$. The result of the fit is presented in Fig. S10(a). As seen, the power law component has the dominant contribution to the electron flux. A similar fit of Eq. (S1) to data, but with f_{e^-} fixed to 0, yields $C_{e^-} = (2.124 \pm 0.010) \times 10^{-3}\,[\mathrm{m}^2\,\mathrm{sr}\,\mathrm{s}\,\mathrm{GeV}]^{-1}$ and $\gamma_{e^-} = -3.186 \pm 0.006$ with $\chi^2/\mathrm{d.o.f.} = 15.2/24$. The result of this fit is presented in Fig. S10(b). Varying the normalisation of the source term f_{e^-} as a free fit parameter does not improve the χ^2 and yields $f_{e^-} = 0.5^{+1.2}_{-0.6}$. As seen in Figs. S10 (a) and (b) the data are consistent both with the charge symmetric positron source term [4] ($f_{e^-} = 1$ in Eq. (S1)) and also with the absence of such a term ($f_{e^-} = 0$). Therefore it is not possible to extract any additional information on the existence and properties of the source term using the electron flux alone.

Time dependence.— We performed fits of Eq. (5) to independent data samples corresponding to a single Bartels rotation [2]. The variation of the χ^2 of these fits is negligible if C_b and γ_b are left to vary freely in the fit or fixed to their average value. Therefore, we fix power law b parameters $C_b = 3.96 \times 10^{-6}\,[\mathrm{m}^2\,\mathrm{sr}\,\mathrm{s}\,\mathrm{GeV}]^{-1}$ and $\gamma_b = -3.14$, which define the spectrum shape at high energies and thus are intrinsically not sensitive to time variations, and determine the remaining parameters for each Bartels rotation. Results are presented in Fig. S11 for (i) the effective modulation parameter φ_{e^-}; (ii) the transition term energy E_t; (iii) the transition term spectral index $\Delta\gamma_t$; (iv) the power law a normalization C_a; and (v) the power law a spectral index γ_a. All parameters are divided by their respective average values to show their relative variation due to time dependent effects. As seen the only parameter which exhibits a significant time variation is φ_{e^-}.

TABLE SI: The electron flux Φ_{e^-} as a function of the energy E at the top of AMS in units of $[\mathrm{m}^2\,\mathrm{sr}\,\mathrm{s}\,\mathrm{GeV}]^{-1}$. Characteristic energy $\tilde{E}$ (i.e. spectrally weighted mean energy in the bin) is given with its systematic error from the energy scale uncertainty. The number of electron events before unfolding, N_{e^-}, is given together with its statistical error from the fit. $\sigma^{e^-}_{\text{stat}}$ is the statistical and $\sigma^{e^-}_{\text{syst}}$ is the total systematic error of the electron flux.

E [GeV]	$\tilde{E}$ [GeV]	N_{e^-}	Φ_{e^-} $\sigma^{e^-}_{\text{stat}}$ $\sigma^{e^-}_{\text{syst}}$
0.50 - 0.65	0.57 ± 0.02	7629 ± 91	$(1.731\ 0.021\ 0.078)\times10^{1}$
0.65 - 0.82	0.73 ± 0.02	86810 ± 301	$(1.710\ 0.006\ 0.063)\times10^{1}$
0.82 - 1.01	0.91 ± 0.03	197265 ± 451	$(1.658\ 0.004\ 0.049)\times10^{1}$
1.01 - 1.22	1.11 ± 0.03	328584 ± 579	$(1.562\ 0.003\ 0.038)\times10^{1}$
1.22 - 1.46	1.33 ± 0.03	494218 ± 709	$(1.391\ 0.002\ 0.028)\times10^{1}$
1.46 - 1.72	1.58 ± 0.04	748885 ± 872	$(1.200\ 0.001\ 0.020)\times10^{1}$
1.72 - 2.00	1.85 ± 0.04	1036495 ± 1027	$(1.027\ 0.001\ 0.015)\times10^{1}$
2.00 - 2.31	2.15 ± 0.05	1302149 ± 1153	$(8.403\ 0.007\ 0.110)\times10^{0}$
2.31 - 2.65	2.47 ± 0.05	1512278 ± 1243	$(6.897\ 0.006\ 0.083)\times10^{0}$
2.65 - 3.00	2.82 ± 0.06	1558061 ± 1264	$(5.504\ 0.004\ 0.064)\times10^{0}$
3.00 - 3.36	3.17 ± 0.06	1540803 ± 1256	$(4.405\ 0.004\ 0.050)\times10^{0}$
3.36 - 3.73	3.54 ± 0.07	1497077 ± 1236	$(3.555\ 0.003\ 0.040)\times10^{0}$
3.73 - 4.12	3.92 ± 0.08	1463912 ± 1222	$(2.859\ 0.002\ 0.032)\times10^{0}$
4.12 - 4.54	4.32 ± 0.08	1437643 ± 1208	$(2.279\ 0.002\ 0.025)\times10^{0}$
4.54 - 5.00	4.76 ± 0.09	1419809 ± 1200	$(1.800\ 0.002\ 0.020)\times10^{0}$
5.00 - 5.49	5.24 ± 0.10	1364759 ± 1176	$(1.409\ 0.001\ 0.016)\times10^{0}$
5.49 - 6.00	5.74 ± 0.11	1273522 ± 1137	$(1.104\ 0.001\ 0.013)\times10^{0}$
6.00 - 6.54	6.26 ± 0.12	1195202 ± 1103	$(8.715\ 0.008\ 0.100)\times10^{-1}$
6.54 - 7.10	6.81 ± 0.13	1074027 ± 1043	$(6.885\ 0.007\ 0.079)\times10^{-1}$
7.10 - 7.69	7.39 ± 0.14	964312 ± 989	$(5.439\ 0.006\ 0.063)\times10^{-1}$
7.69 - 8.30	7.99 ± 0.15	843948 ± 924	$(4.309\ 0.005\ 0.051)\times10^{-1}$
8.30 - 8.95	8.62 ± 0.16	755410 ± 874	$(3.415\ 0.004\ 0.040)\times10^{-1}$
8.95 - 9.62	9.28 ± 0.18	661333 ± 817	$(2.747\ 0.003\ 0.033)\times10^{-1}$
9.62 - 10.32	9.96 ± 0.19	583806 ± 768	$(2.204\ 0.003\ 0.026)\times10^{-1}$
10.32 - 11.04	10.67 ± 0.20	504176 ± 712	$(1.779\ 0.003\ 0.022)\times10^{-1}$
11.04 - 11.80	11.41 ± 0.22	448010 ± 672	$(1.438\ 0.002\ 0.018)\times10^{-1}$
11.80 - 12.59	12.19 ± 0.23	395528 ± 630	$(1.170\ 0.002\ 0.014)\times10^{-1}$
12.59 - 13.41	12.99 ± 0.25	349454 ± 593	$(9.557\ 0.016\ 0.118)\times10^{-2}$
13.41 - 14.25	13.82 ± 0.26	306269 ± 555	$(7.849\ 0.014\ 0.098)\times10^{-2}$
14.25 - 15.14	14.69 ± 0.28	277278 ± 528	$(6.439\ 0.012\ 0.081)\times10^{-2}$
15.14 - 16.05	15.59 ± 0.29	244941 ± 496	$(5.316\ 0.011\ 0.067)\times10^{-2}$
16.05 - 17.00	16.52 ± 0.31	220144 ± 470	$(4.382\ 0.009\ 0.056)\times10^{-2}$
17.00 - 17.98	17.48 ± 0.33	198307 ± 446	$(3.659\ 0.008\ 0.047)\times10^{-2}$
17.98 - 18.99	18.48 ± 0.35	180080 ± 425	$(3.057\ 0.007\ 0.039)\times10^{-2}$
18.99 - 20.04	19.51 ± 0.37	165546 ± 408	$(2.573\ 0.006\ 0.033)\times10^{-2}$
20.04 - 21.13	20.58 ± 0.39	147538 ± 385	$(2.146\ 0.006\ 0.028)\times10^{-2}$
21.13 - 22.25	21.68 ± 0.41	131846 ± 364	$(1.804\ 0.005\ 0.024)\times10^{-2}$
22.25 - 23.42	22.83 ± 0.43	119578 ± 346	$(1.524\ 0.004\ 0.020)\times10^{-2}$

Continued on next page

TABLE SI – *(Continued).*

E [GeV]	$\tilde{E}$ [GeV]	N_{e^-}	Φ_{e^-} $\sigma^{e^-}_{\mathrm{stat}}$ $\sigma^{e^-}_{\mathrm{syst}}$
23.42 - 24.62	24.01 ± 0.45	106414 ± 327	(1.291 0.004 0.017)$\times 10^{-2}$
24.62 - 25.90	25.25 ± 0.48	98745 ± 315	(1.099 0.004 0.015)$\times 10^{-2}$
25.90 - 27.25	26.56 ± 0.50	89203 ± 299	(9.236 0.031 0.123)$\times 10^{-3}$
27.25 - 28.68	27.95 ± 0.53	80344 ± 284	(7.841 0.028 0.105)$\times 10^{-3}$
28.68 - 30.21	29.43 ± 0.56	72576 ± 270	(6.622 0.025 0.089)$\times 10^{-3}$
30.21 - 31.82	31.00 ± 0.59	63528 ± 253	(5.530 0.022 0.074)$\times 10^{-3}$
31.82 - 33.53	32.66 ± 0.62	57191 ± 240	(4.685 0.020 0.063)$\times 10^{-3}$
33.53 - 35.36	34.43 ± 0.65	51322 ± 227	(3.947 0.017 0.053)$\times 10^{-3}$
35.36 - 37.31	36.32 ± 0.69	45871 ± 215	(3.311 0.015 0.045)$\times 10^{-3}$
37.31 - 39.39	38.33 ± 0.72	41312 ± 204	(2.806 0.014 0.038)$\times 10^{-3}$
39.39 - 41.61	40.48 ± 0.77	36784 ± 192	(2.343 0.012 0.032)$\times 10^{-3}$
41.61 - 44.00	42.78 ± 0.81	32850 ± 182	(1.951 0.011 0.027)$\times 10^{-3}$
44.00 - 46.57	45.26 ± 0.86	29514 ± 172	(1.635 0.010 0.022)$\times 10^{-3}$
46.57 - 49.33	47.92 ± 0.91	26470 ± 163	(1.367 0.008 0.019)$\times 10^{-3}$
49.33 - 52.33	50.80 ± 0.96	23477 ± 154	(1.119 0.007 0.015)$\times 10^{-3}$
52.33 - 55.58	53.92 ± 1.02	21067 ± 146	(9.297 0.064 0.128)$\times 10^{-4}$
55.58 - 59.13	57.32 ± 1.08	18928 ± 138	(7.663 0.056 0.106)$\times 10^{-4}$
59.13 - 63.02	61.03 ± 1.16	16677 ± 130	(6.191 0.048 0.086)$\times 10^{-4}$
63.02 - 67.30	65.11 ± 1.23	15006 ± 123	(5.072 0.042 0.070)$\times 10^{-4}$
67.30 - 72.05	69.62 ± 1.32	13327 ± 116	(4.075 0.035 0.056)$\times 10^{-4}$
72.05 - 77.37	74.65 ± 1.41	12066 ± 110	(3.296 0.030 0.046)$\times 10^{-4}$
77.37 - 83.36	80.29 ± 1.52	10716 ± 104	(2.613 0.025 0.036)$\times 10^{-4}$
83.36 - 90.19	86.69 ± 1.64	9536 ± 98	(2.048 0.021 0.028)$\times 10^{-4}$
90.19 - 98.08	94.02 ± 1.78	8457 ± 93	(1.579 0.017 0.022)$\times 10^{-4}$
98.1 - 107.3	102.6 ± 1.9	7589 ± 89	(1.214 0.014 0.017)$\times 10^{-4}$
107.3 - 118.4	112.7 ± 2.1	6605 ± 82	(8.891 0.111 0.124)$\times 10^{-5}$
118.4 - 132.1	125.0 ± 2.4	5882 ± 78	(6.460 0.086 0.090)$\times 10^{-5}$
132.1 - 148.8	140.1 ± 2.7	4805 ± 70	(4.531 0.066 0.065)$\times 10^{-5}$
148.8 - 169.9	158.9 ± 3.0	4020 ± 64	(3.010 0.048 0.043)$\times 10^{-5}$
169.9 - 197.7	183.1 ± 3.5	3221 ± 58	(1.853 0.034 0.027)$\times 10^{-5}$
197.7 - 237.2	216.2 ± 4.2	2331 ± 49	(1.075 0.023 0.017)$\times 10^{-5}$
237.2 - 290.0	261.8 ± 5.1	1706 ± 43	(5.978 0.149 0.100)$\times 10^{-6}$
290.0 - 370.0	326.8 ± 6.4	1161 ± 36	(3.129 0.096 0.055)$\times 10^{-6}$
370.0 - 500.0	428.5 ± 8.6	747 ± 29	(1.278 0.050 0.026)$\times 10^{-6}$
500.0 - 700.0	588.8 ± 12.2	392 ± 23	(4.560 0.268 0.119)$\times 10^{-7}$
700.0 - 1000.0	832.3 ± 18.3	214 ± 19	(1.771 0.158 0.063)$\times 10^{-7}$
1000.0 - 1400.0	1177.7 ± 28.6	68 ± 12	(4.123 0.700 0.220)$\times 10^{-8}$

TABLE SII: The combined (electron + positron) flux ($\Phi_{e^-} + \Phi_{e^+}$) in units of $[\mathrm{m}^2\,\mathrm{sr}\,\mathrm{s}\,\mathrm{GeV}]^{-1}$ and positron fraction ($\mathrm{PF} \equiv \Phi_{e^+}/(\Phi_{e^-} + \Phi_{e^+})$) as a function of the energy E at the top of AMS. ($\Phi_{e^-} + \Phi_{e^+}$) and PF are calculated from the electron flux in this Letter and the positron flux from Ref. [4]. $\sigma_{\mathrm{stat}}^{e^-+e^+}$ and $\sigma_{\mathrm{syst}}^{e^-+e^+}$ are the statistical error and the total systematic error of the combined (electron + positron) flux. $\sigma_{\mathrm{stat}}^{\mathrm{PF}}$ and $\sigma_{\mathrm{syst}}^{\mathrm{PF}}$ are the statistical error and the total systematic error of the positron fraction. The systematic errors of the combined (electron + positron) flux and the positron fraction account for correlations related to the calculation of the acceptance.

E [GeV]	($\Phi_{e^-} + \Phi_{e^+}$)	$\sigma_{\mathrm{stat}}^{e^-+e^+}$	$\sigma_{\mathrm{syst}}^{e^-+e^+}$	PF	$\sigma_{\mathrm{stat}}^{\mathrm{PF}}$	$\sigma_{\mathrm{syst}}^{\mathrm{PF}}$
0.50 - 0.65	(1.998	0.023	0.088)$\times 10^{1}$	(1.309	0.049	0.033)$\times 10^{-1}$
0.65 - 0.82	(1.967	0.007	0.071)$\times 10^{1}$	(1.295	0.013	0.021)$\times 10^{-1}$
0.82 - 1.01	(1.885	0.004	0.055)$\times 10^{1}$	(1.188	0.008	0.010)$\times 10^{-1}$
1.01 - 1.22	(1.754	0.003	0.042)$\times 10^{1}$	(1.090	0.006	0.007)$\times 10^{-1}$
1.22 - 1.46	(1.544	0.002	0.030)$\times 10^{1}$	(9.919	0.044	0.052)$\times 10^{-2}$
1.46 - 1.72	(1.320	0.001	0.022)$\times 10^{1}$	(9.081	0.034	0.040)$\times 10^{-2}$
1.72 - 2.00	(1.119	0.001	0.016)$\times 10^{1}$	(8.316	0.027	0.030)$\times 10^{-2}$
2.00 - 2.31	(9.103	0.008	0.118)$\times 10^{0}$	(7.735	0.024	0.027)$\times 10^{-2}$
2.31 - 2.65	(7.431	0.006	0.089)$\times 10^{0}$	(7.221	0.021	0.025)$\times 10^{-2}$
2.65 - 3.00	(5.903	0.005	0.068)$\times 10^{0}$	(6.783	0.021	0.023)$\times 10^{-2}$
3.00 - 3.36	(4.708	0.004	0.053)$\times 10^{0}$	(6.455	0.020	0.022)$\times 10^{-2}$
3.36 - 3.73	(3.789	0.003	0.042)$\times 10^{0}$	(6.196	0.020	0.021)$\times 10^{-2}$
3.73 - 4.12	(3.040	0.002	0.034)$\times 10^{0}$	(5.972	0.020	0.020)$\times 10^{-2}$
4.12 - 4.54	(2.418	0.002	0.027)$\times 10^{0}$	(5.759	0.020	0.019)$\times 10^{-2}$
4.54 - 5.00	(1.907	0.002	0.021)$\times 10^{0}$	(5.620	0.020	0.018)$\times 10^{-2}$
5.00 - 5.49	(1.491	0.001	0.017)$\times 10^{0}$	(5.517	0.020	0.018)$\times 10^{-2}$
5.49 - 6.00	(1.166	0.001	0.013)$\times 10^{0}$	(5.391	0.021	0.017)$\times 10^{-2}$
6.00 - 6.54	(9.207	0.008	0.105)$\times 10^{-1}$	(5.353	0.021	0.017)$\times 10^{-2}$
6.54 - 7.10	(7.274	0.007	0.084)$\times 10^{-1}$	(5.353	0.022	0.017)$\times 10^{-2}$
7.10 - 7.69	(5.741	0.006	0.067)$\times 10^{-1}$	(5.260	0.023	0.017)$\times 10^{-2}$
7.69 - 8.30	(4.550	0.005	0.053)$\times 10^{-1}$	(5.289	0.025	0.017)$\times 10^{-2}$
8.30 - 8.95	(3.605	0.004	0.043)$\times 10^{-1}$	(5.272	0.026	0.017)$\times 10^{-2}$
8.95 - 9.62	(2.900	0.003	0.034)$\times 10^{-1}$	(5.277	0.028	0.018)$\times 10^{-2}$
9.62 - 10.32	(2.329	0.003	0.028)$\times 10^{-1}$	(5.333	0.030	0.018)$\times 10^{-2}$
10.32 - 11.04	(1.880	0.003	0.023)$\times 10^{-1}$	(5.353	0.033	0.019)$\times 10^{-2}$
11.04 - 11.80	(1.521	0.002	0.019)$\times 10^{-1}$	(5.456	0.035	0.019)$\times 10^{-2}$
11.80 - 12.59	(1.239	0.002	0.015)$\times 10^{-1}$	(5.581	0.037	0.020)$\times 10^{-2}$
12.59 - 13.41	(1.012	0.002	0.013)$\times 10^{-1}$	(5.595	0.040	0.020)$\times 10^{-2}$
13.41 - 14.25	(8.313	0.015	0.103)$\times 10^{-2}$	(5.581	0.043	0.020)$\times 10^{-2}$
14.25 - 15.14	(6.826	0.013	0.085)$\times 10^{-2}$	(5.656	0.045	0.020)$\times 10^{-2}$
15.14 - 16.05	(5.642	0.011	0.071)$\times 10^{-2}$	(5.776	0.048	0.021)$\times 10^{-2}$
16.05 - 17.00	(4.654	0.010	0.059)$\times 10^{-2}$	(5.833	0.051	0.021)$\times 10^{-2}$
17.00 - 17.98	(3.888	0.009	0.050)$\times 10^{-2}$	(5.891	0.054	0.021)$\times 10^{-2}$
17.98 - 18.99	(3.250	0.007	0.042)$\times 10^{-2}$	(5.940	0.057	0.021)$\times 10^{-2}$
18.99 - 20.04	(2.740	0.007	0.035)$\times 10^{-2}$	(6.075	0.060	0.021)$\times 10^{-2}$
20.04 - 21.13	(2.292	0.006	0.030)$\times 10^{-2}$	(6.339	0.065	0.022)$\times 10^{-2}$

Continued on next page

TABLE SII – *(Continued)*.

E [GeV]	$(\Phi_{e^-}+\Phi_{e^+})$	$\sigma_{\text{stat}}^{e^-+e^+}$	$\sigma_{\text{syst}}^{e^-+e^+}$	PF	$\sigma_{\text{stat}}^{\text{PF}}$	$\sigma_{\text{syst}}^{\text{PF}}$
21.13 - 22.25	(1.925	0.005	0.025)$\times10^{-2}$	(6.298	0.068	0.022)$\times10^{-2}$
22.25 - 23.42	(1.626	0.005	0.021)$\times10^{-2}$	(6.252	0.072	0.022)$\times10^{-2}$
23.42 - 24.62	(1.381	0.004	0.018)$\times10^{-2}$	(6.529	0.077	0.024)$\times10^{-2}$
24.62 - 25.90	(1.176	0.004	0.016)$\times10^{-2}$	(6.495	0.080	0.024)$\times10^{-2}$
25.90 - 27.25	(9.911	0.032	0.132)$\times10^{-3}$	(6.808	0.086	0.026)$\times10^{-2}$
27.25 - 28.68	(8.416	0.029	0.112)$\times10^{-3}$	(6.820	0.091	0.027)$\times10^{-2}$
28.68 - 30.21	(7.128	0.026	0.095)$\times10^{-3}$	(7.093	0.097	0.029)$\times10^{-2}$
30.21 - 31.82	(5.957	0.023	0.080)$\times10^{-3}$	(7.164	0.105	0.030)$\times10^{-2}$
31.82 - 33.53	(5.053	0.020	0.068)$\times10^{-3}$	(7.274	0.111	0.031)$\times10^{-2}$
33.53 - 35.36	(4.260	0.018	0.058)$\times10^{-3}$	(7.330	0.118	0.032)$\times10^{-2}$
35.36 - 37.31	(3.587	0.016	0.049)$\times10^{-3}$	(7.669	0.127	0.035)$\times10^{-2}$
37.31 - 39.39	(3.039	0.014	0.041)$\times10^{-3}$	(7.652	0.134	0.036)$\times10^{-2}$
39.39 - 41.61	(2.543	0.013	0.035)$\times10^{-3}$	(7.870	0.143	0.038)$\times10^{-2}$
41.61 - 44.00	(2.123	0.011	0.029)$\times10^{-3}$	(8.105	0.154	0.041)$\times10^{-2}$
44.00 - 46.57	(1.779	0.010	0.024)$\times10^{-3}$	(8.115	0.163	0.042)$\times10^{-2}$
46.57 - 49.33	(1.499	0.009	0.021)$\times10^{-3}$	(8.811	0.178	0.047)$\times10^{-2}$
49.33 - 52.33	(1.222	0.008	0.017)$\times10^{-3}$	(8.406	0.186	0.047)$\times10^{-2}$
52.33 - 55.58	(1.018	0.007	0.014)$\times10^{-3}$	(8.689	0.199	0.051)$\times10^{-2}$
55.58 - 59.13	(8.419	0.059	0.116)$\times10^{-4}$	(8.967	0.213	0.054)$\times10^{-2}$
59.13 - 63.02	(6.803	0.051	0.094)$\times10^{-4}$	(8.978	0.228	0.056)$\times10^{-2}$
63.02 - 67.30	(5.622	0.044	0.078)$\times10^{-4}$	(9.775	0.249	0.063)$\times10^{-2}$
67.30 - 72.05	(4.511	0.038	0.062)$\times10^{-4}$	(9.670	0.263	0.066)$\times10^{-2}$
72.05 - 77.37	(3.678	0.032	0.051)$\times10^{-4}$	(1.039	0.028	0.007)$\times10^{-1}$
77.37 - 83.36	(2.914	0.027	0.040)$\times10^{-4}$	(1.033	0.030	0.008)$\times10^{-1}$
83.36 - 90.19	(2.299	0.023	0.032)$\times10^{-4}$	(1.091	0.033	0.009)$\times10^{-1}$
90.19 - 98.08	(1.782	0.019	0.025)$\times10^{-4}$	(1.142	0.036	0.010)$\times10^{-1}$
98.1 - 107.3	(1.360	0.015	0.019)$\times10^{-4}$	(1.073	0.040	0.009)$\times10^{-1}$
107.3 - 118.4	(1.006	0.012	0.014)$\times10^{-4}$	(1.165	0.044	0.010)$\times10^{-1}$
118.4 - 132.1	(7.328	0.094	0.103)$\times10^{-5}$	(1.183	0.047	0.010)$\times10^{-1}$
132.1 - 148.8	(5.231	0.073	0.075)$\times10^{-5}$	(1.337	0.053	0.012)$\times10^{-1}$
148.8 - 169.9	(3.469	0.053	0.050)$\times10^{-5}$	(1.323	0.058	0.012)$\times10^{-1}$
169.9 - 197.7	(2.173	0.037	0.032)$\times10^{-5}$	(1.472	0.068	0.014)$\times10^{-1}$
197.7 - 237.2	(1.263	0.025	0.020)$\times10^{-5}$	(1.481	0.080	0.017)$\times10^{-1}$
237.2 - 290.0	(7.136	0.168	0.119)$\times10^{-6}$	(1.621	0.097	0.023)$\times10^{-1}$
290.0 - 370.0	(3.706	0.108	0.065)$\times10^{-6}$	(1.557	0.120	0.028)$\times10^{-1}$
370.0 - 500.0	(1.527	0.058	0.031)$\times10^{-6}$	(1.630	0.166	0.050)$\times10^{-1}$
500.0 - 700.0	(5.391	0.316	0.153)$\times10^{-7}$	(1.541	0.274	0.130)$\times10^{-1}$
700.0 - 1000.0	(1.963	0.192	0.080)$\times10^{-7}$	(9.802	5.052	2.181)$\times10^{-2}$

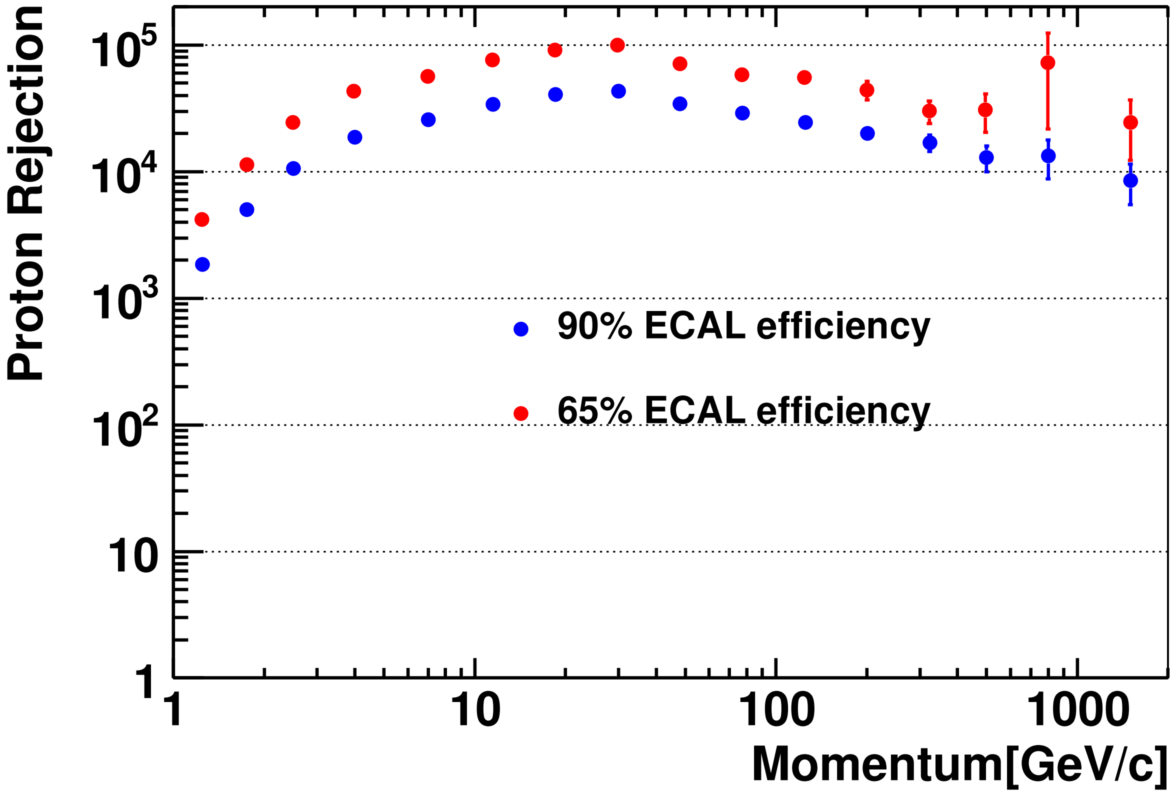

FIG. S1. Comparison of the measured proton rejection for two cuts on the Λ_{ECAL}: with nominal 90% (blue circles, taken from Ref. [20]) and tighter 65% (red circles) selection efficiencies. A total of 1.03 billion proton events are used in the momentum range $[1-2000]$ GeV/c in this analysis.

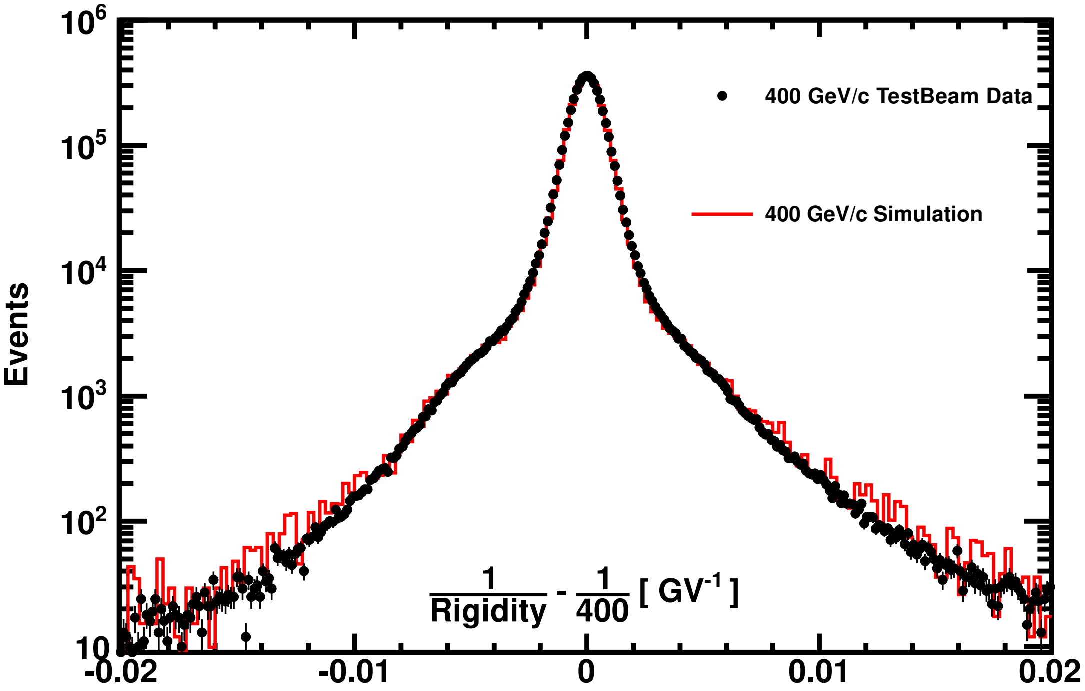

FIG. S2. The comparison between data and the Monte Carlo simulation of the inverse rigidity measured by the tracker for 400 GV test beam protons. As seen, the Monte Carlo simulation describes not only detector resolution effects (the central core of the distribution) but also the various interactions with the detector materials including multiple, large angle, elastic, and quasi-elastic scattering (tails of the distribution). Note that the agreement between the data and the Monte Carlo simulation extends over five orders of magnitude.

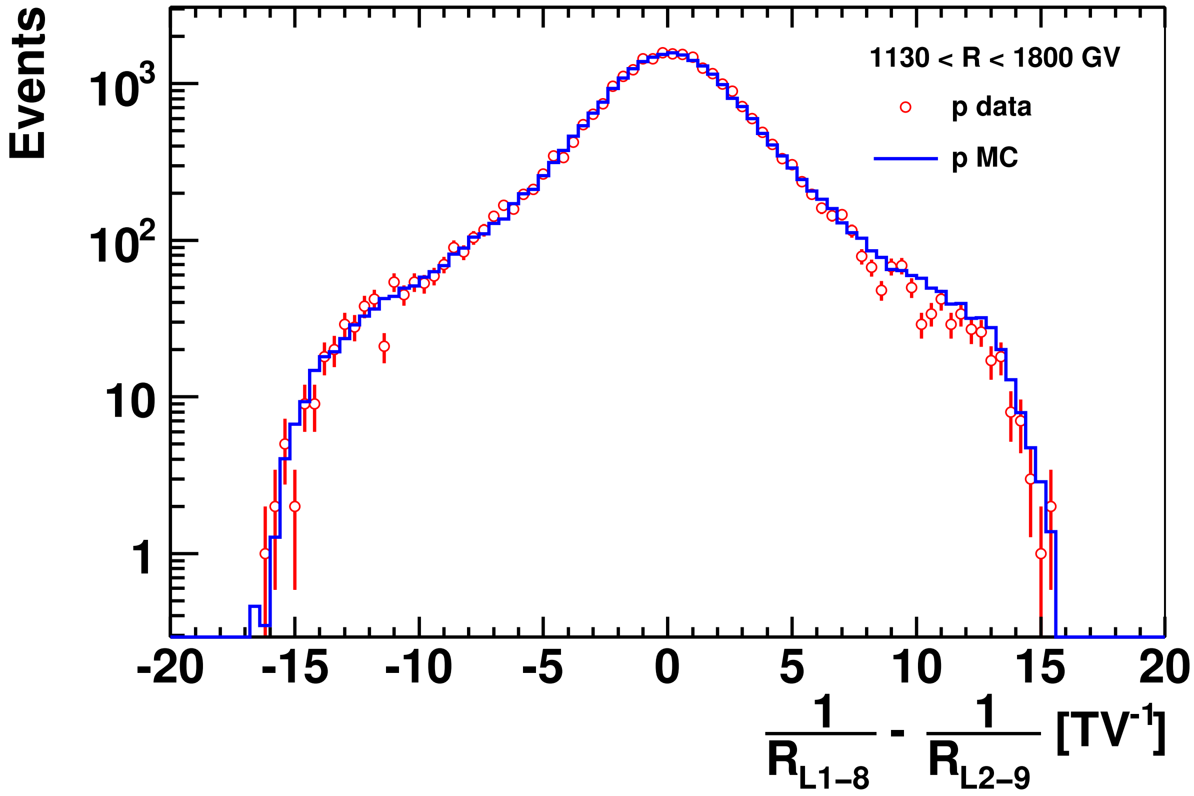

FIG. S3. The difference of the inverse rigidities measured with the upper (layers $L1$-$L8$) and the lower (layers $L2$-$L9$) parts of the tracker for the cosmic ray proton data collected on the Space Station and the Monte Carlo simulation for the rigidity range $[1130-1800]$ GV, close to the tracker tracker maximum detectable rigidity (MDR) of 2 TV. As seen, the distribution of the difference of these inverse rigidities is in good agreement with the Monte Carlo simulation and is centered at zero.

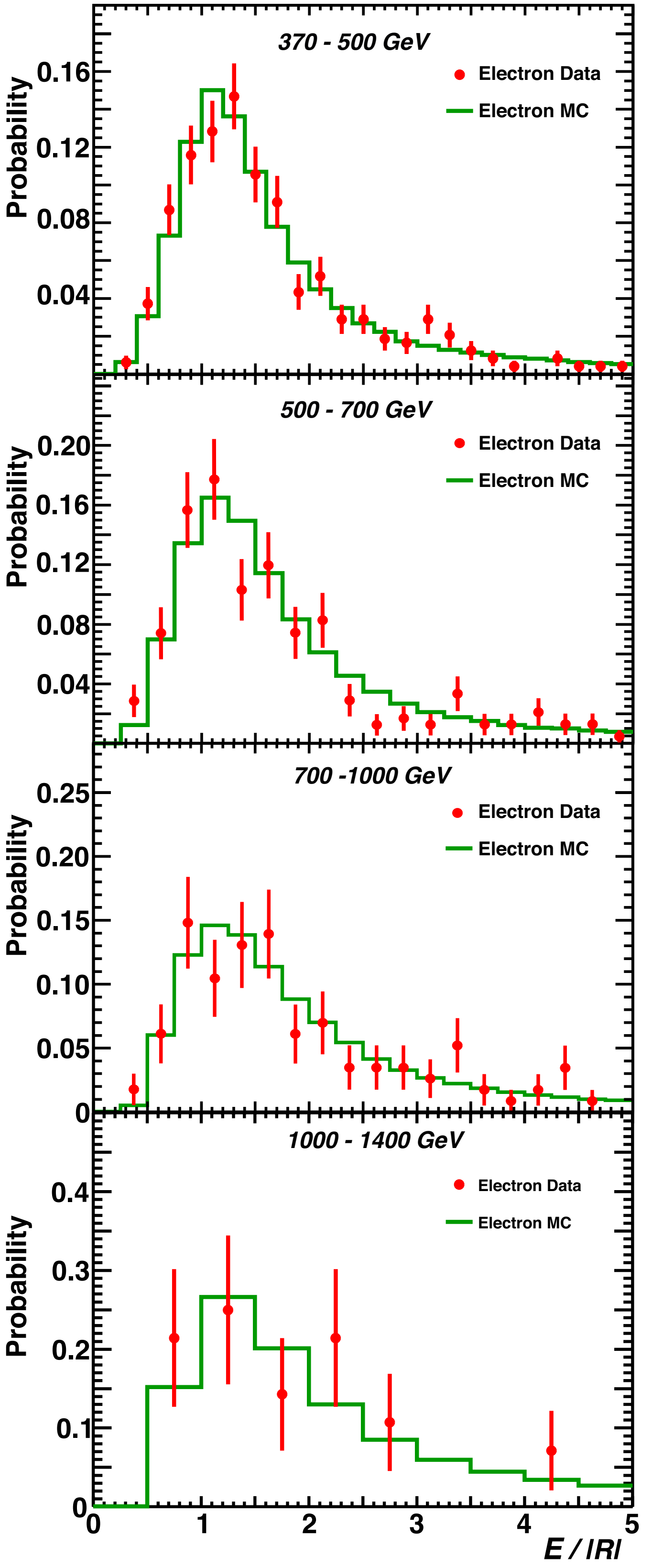

FIG. S4. Comparison of the $E/|R|$ distribution for electrons in the data and the Monte Carlo simulation. As seen, the simulation accurately reproduces the data in different energy bins.

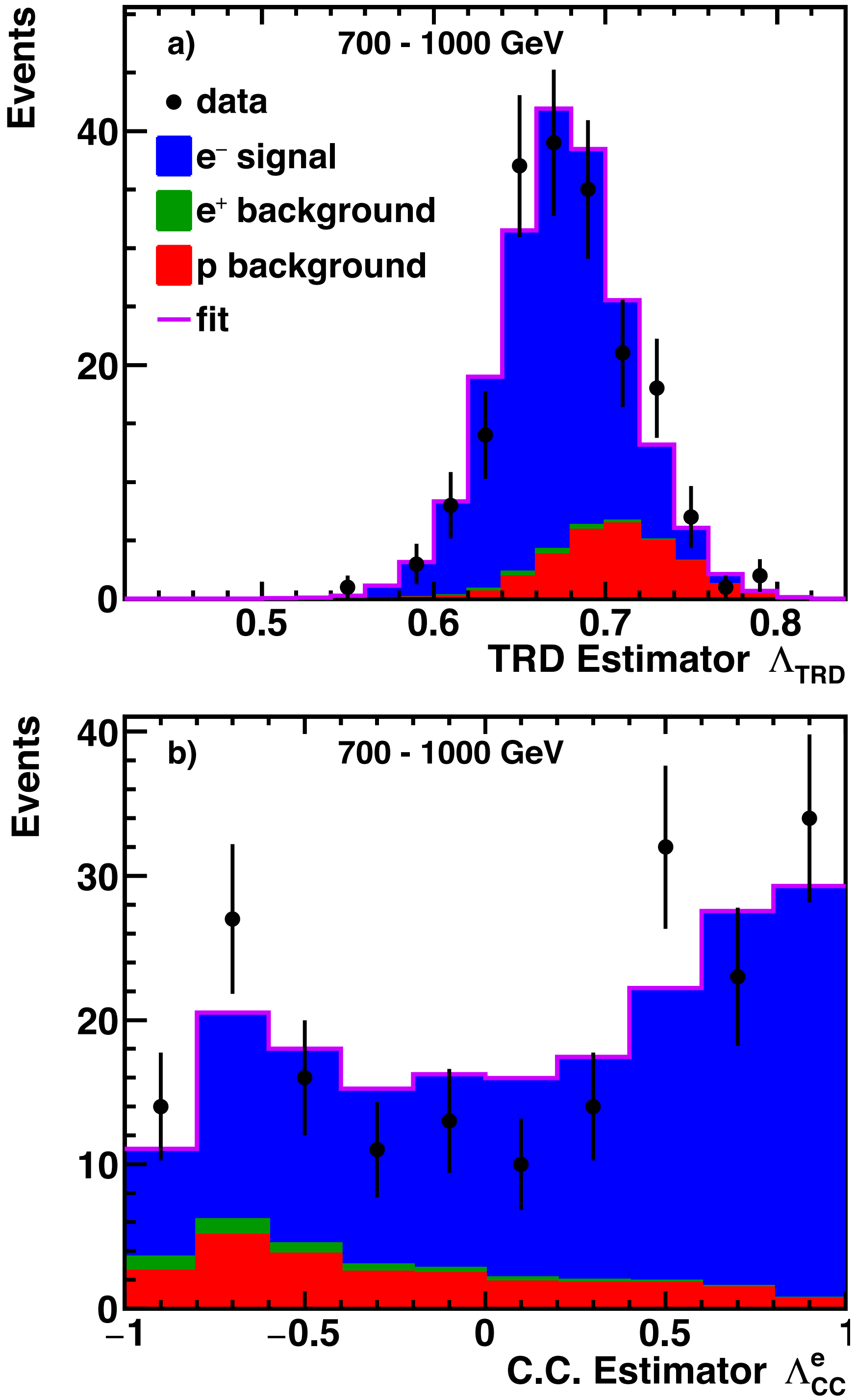

FIG. S5. An illustration of the fit to the data in the energy bin $[700 - 1000]$ GeV for the negative rigidity data sample. The projections of the 2D data distribution (black data points) to the (a) $\Lambda_{\rm TRD}$ and (b) $\Lambda^{e}_{\rm CC}$ axes are shown together with the signal and background contributions: the electron signal (blue), the charge confusion positron background (green, nearly invisible in (a) and (b)), and the charge confusion proton background (red). The projection onto the $\Lambda_{\rm TRD}$ axis uses selection cut $\Lambda^{e}_{\rm CC} > -0.4$ and the projection onto the $\Lambda^{e}_{\rm CC}$ axis uses selection cut $\Lambda_{\rm TRD} < 0.7$. These cuts are applied for demonstration purposes only, such that ~80% of the signal events quoted in Table SI are shown in these plots.

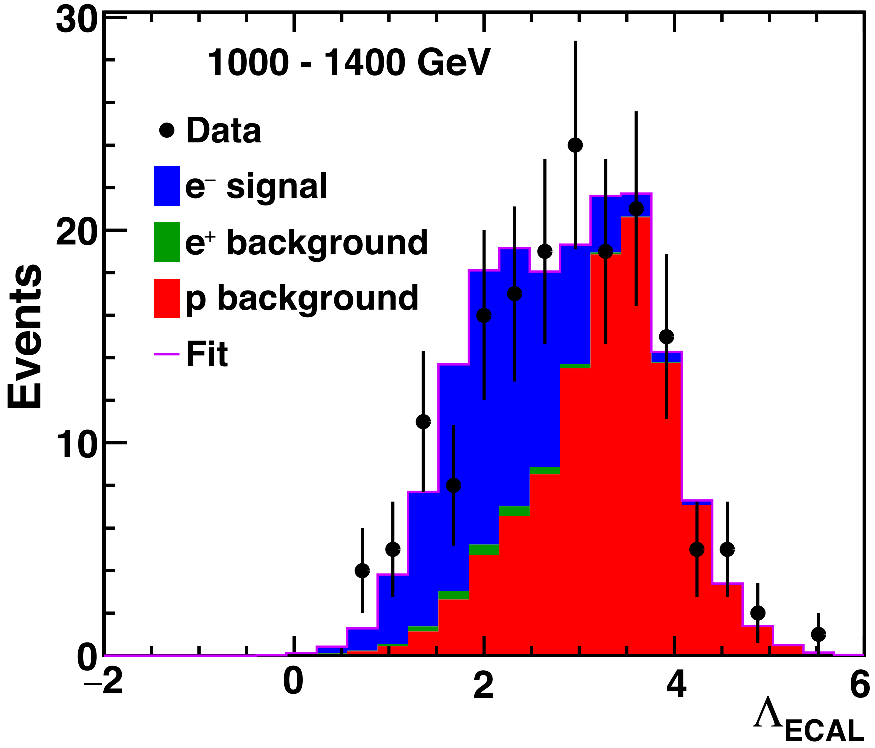

FIG. S6. The fit to the data in the energy bin $[1000-1400]$ GeV for the negative rigidity data sample. The Λ_{ECAL} distribution of the selected data events (black data points) is shown together with the signal and background contributions: the electron signal (blue), the charge confusion positron background (green, nearly invisible), and the charge confusion proton background (red).

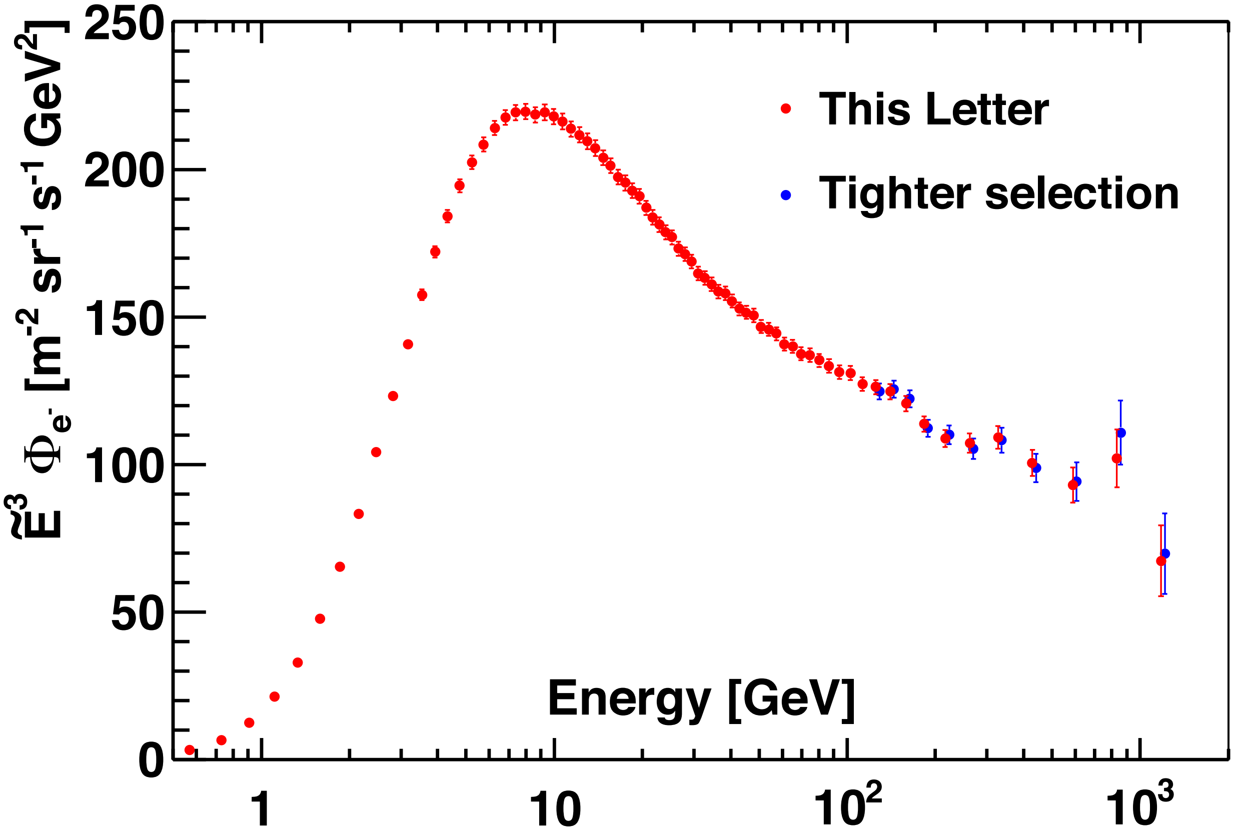

FIG. S7. Comparison of the data presented in this Letter (red data points) with the results of a tighter ECAL cut on the electron selection for energy bins starting from 118.4 GeV (blue data points). The tighter ECAL cut has a signal efficiency of 65% instead of the nominal 90% (see Fig. S1). It reduces the proton background by a factor ∼3 compared to the nominal one described in the Letter. For display purposes, the results of the tighter cut are slightly offset horizontally. As seen, both selections yield consistent results.

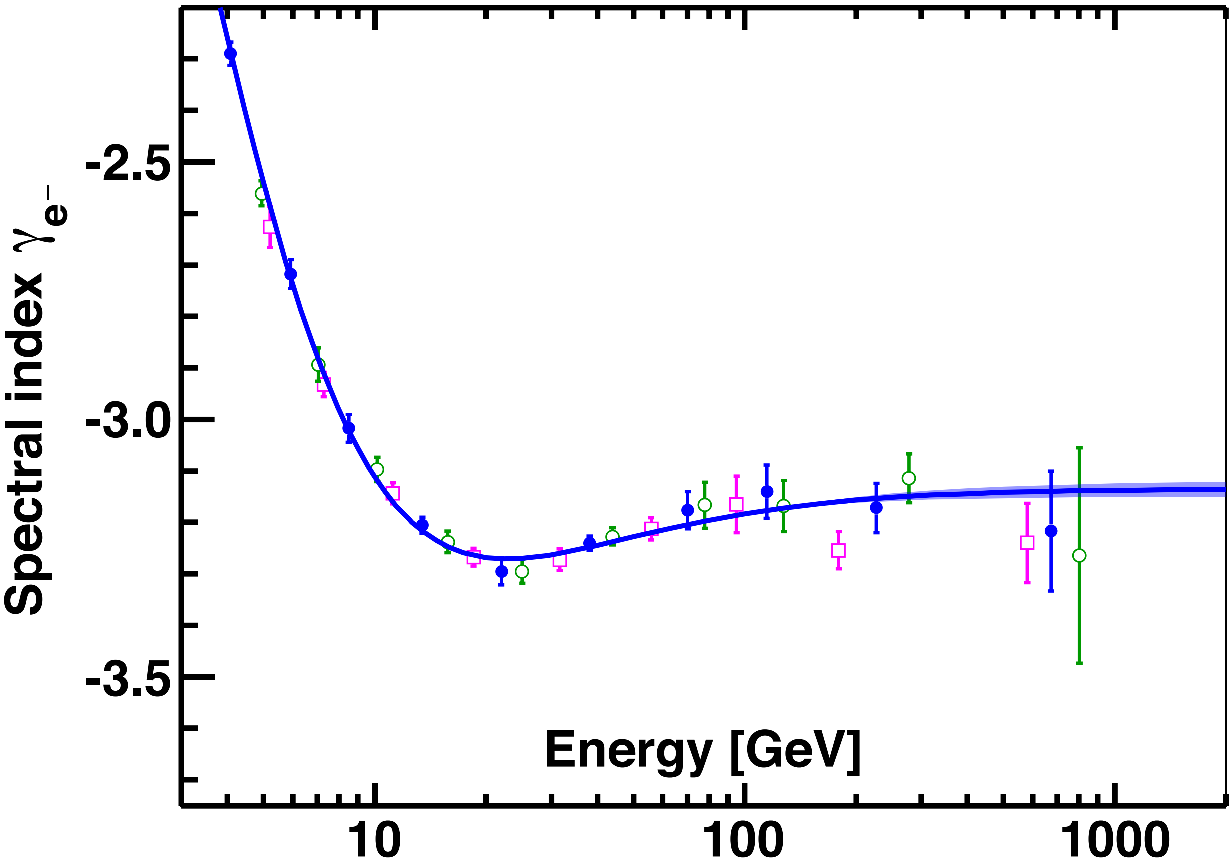

FIG. S8. The electron flux spectral index in non-overlapping energy intervals. Blue data points correspond to the energy ranges in the text (see Fig. 3(a) in the main text), the open magenta squares correspond to the energy ranges shifted by one or two energy bins to the left, and the open green circles correspond to the energy ranges shifted by one or two bins to the right. The blue band represents the 68% C.L. interval of the spectral index from the fit to the electron flux using Eq. (5).

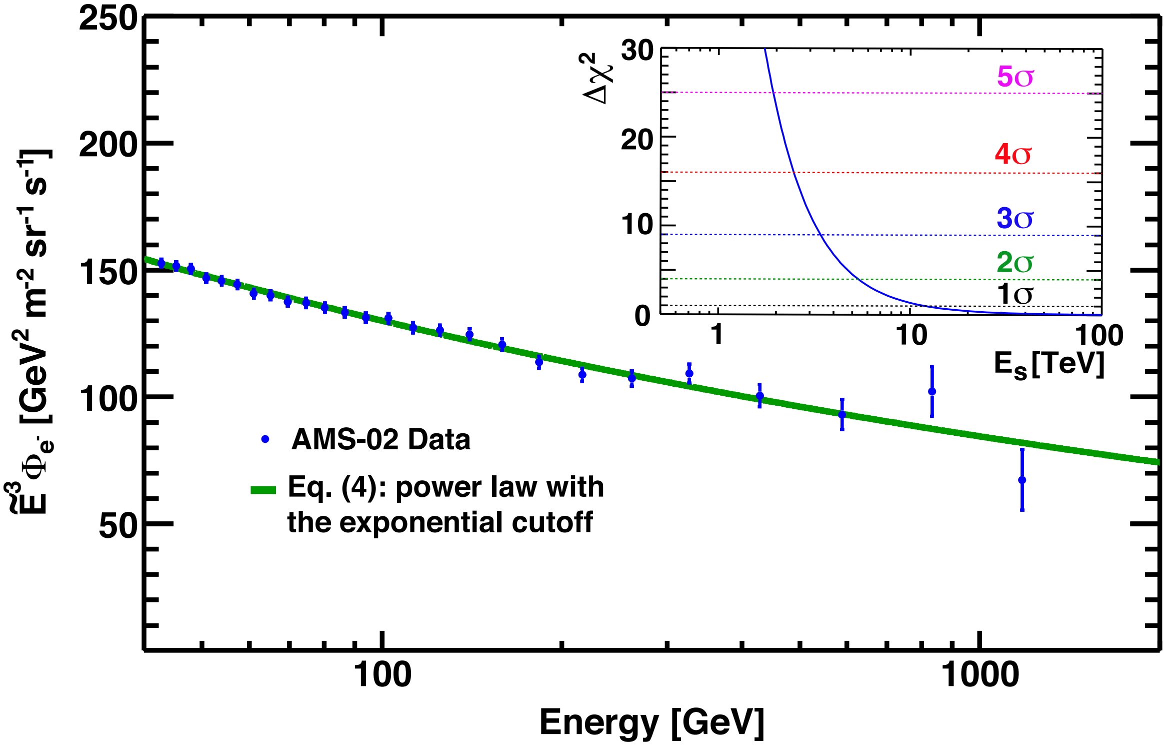

FIG. S9. The fit of Eq. (4) to the electron flux data in the energy range $[41.61 - 1400]$ GeV. The insert shows the study of the significance of the $1/E_s$ measurement by varying all three fit parameters in Eq. (4) to find the minimal $\Delta\chi^2$ corresponding to E_s values from 1 to 100 TeV. The blue curve shows the dependence of $\Delta\chi^2$ on E_s and the horizontal dashed lines show different significance levels from 1 to 5σ. As seen, E_s values below 1.9 TeV are excluded at the 5σ level.

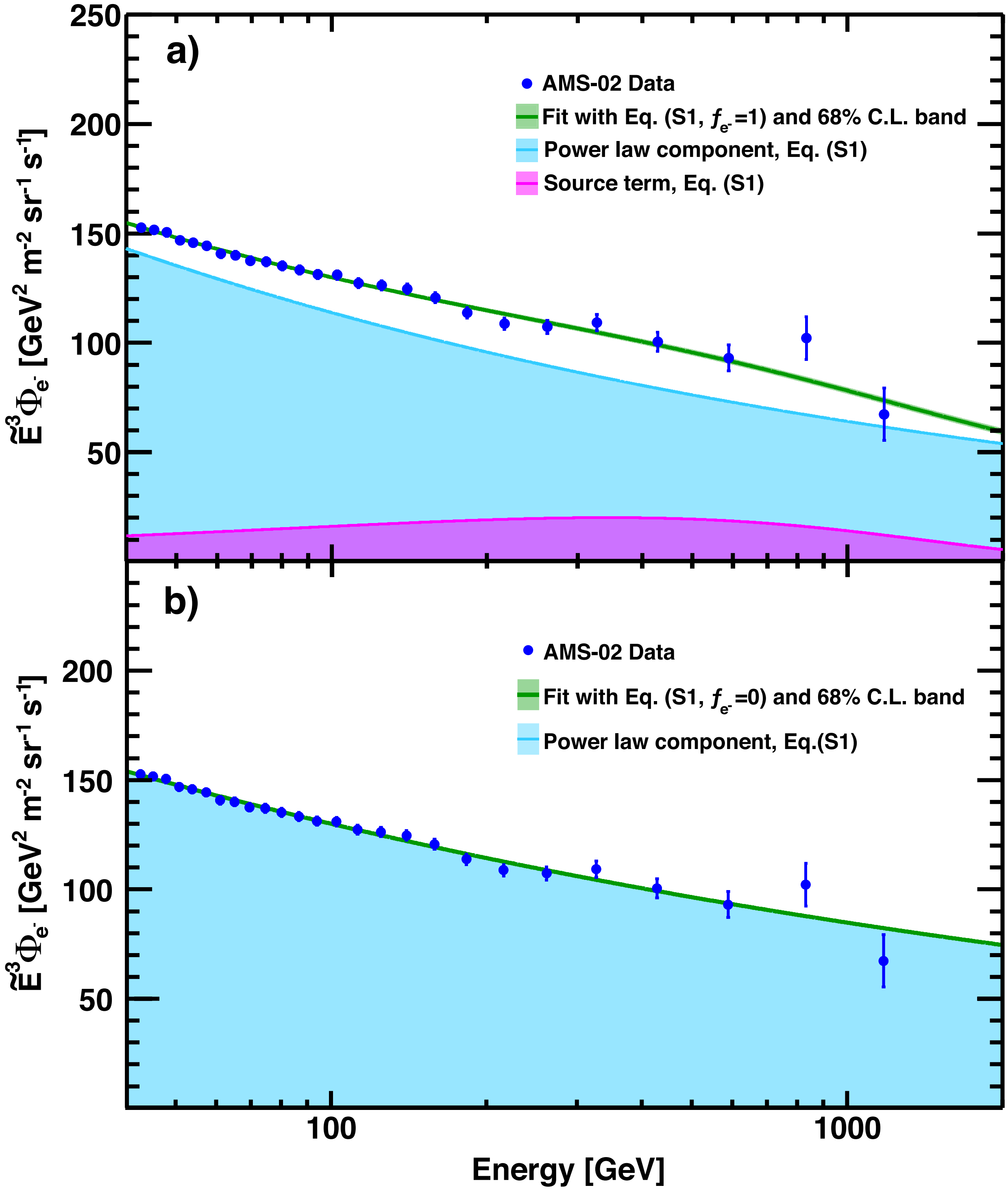

FIG. S10. (a) The fit of Eq. (S1, $f_{e^-} = 1$) to the electron flux data in the energy range $[41.61 - 1400]$ GeV with the 68% C.L. (green band). The source term contribution, identical to that of positrons, is represented by the magenta area and the power law component by the blue area. (b) The fit of Eq. (S1, $f_{e^-} = 0$) to the electron flux data in the energy range $[41.61 - 1400]$ GeV with the 68% C.L. (green band). The power law component is represented by the blue area.

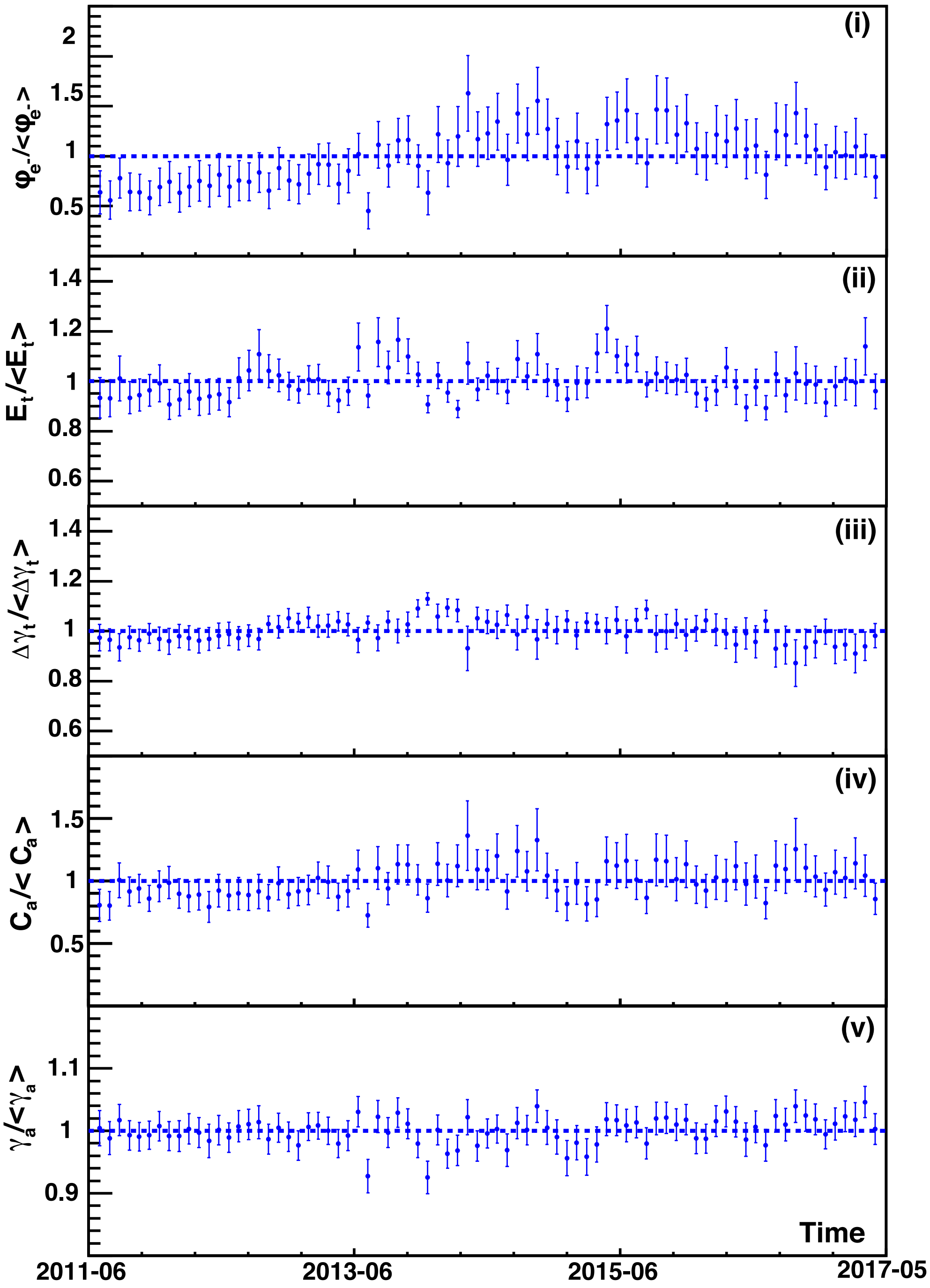

FIG. S11. The time dependence of the Eq. (5) fit parameters for the time period from May 2011 to May 2017. The results of fits of Eq. (5) to the data samples each corresponding to a single Bartels rotation [2] for
(i) the effective modulation parameter φ_{e^-};
(ii) the transition term energy E_t;
(iii) the transition term spectral index $\Delta\gamma_t$;
(iv) the power law a normalization C_a; and
(v) the power law a spectral index γ_a.
All parameters are divided by their respective average values to indicate their relative variation due to time dependent effects.